22/ 116

UCRL-ID-112606

Handbook of Actuators and Edge Alignment Sensors

Debra A. Krulewich

November 1992

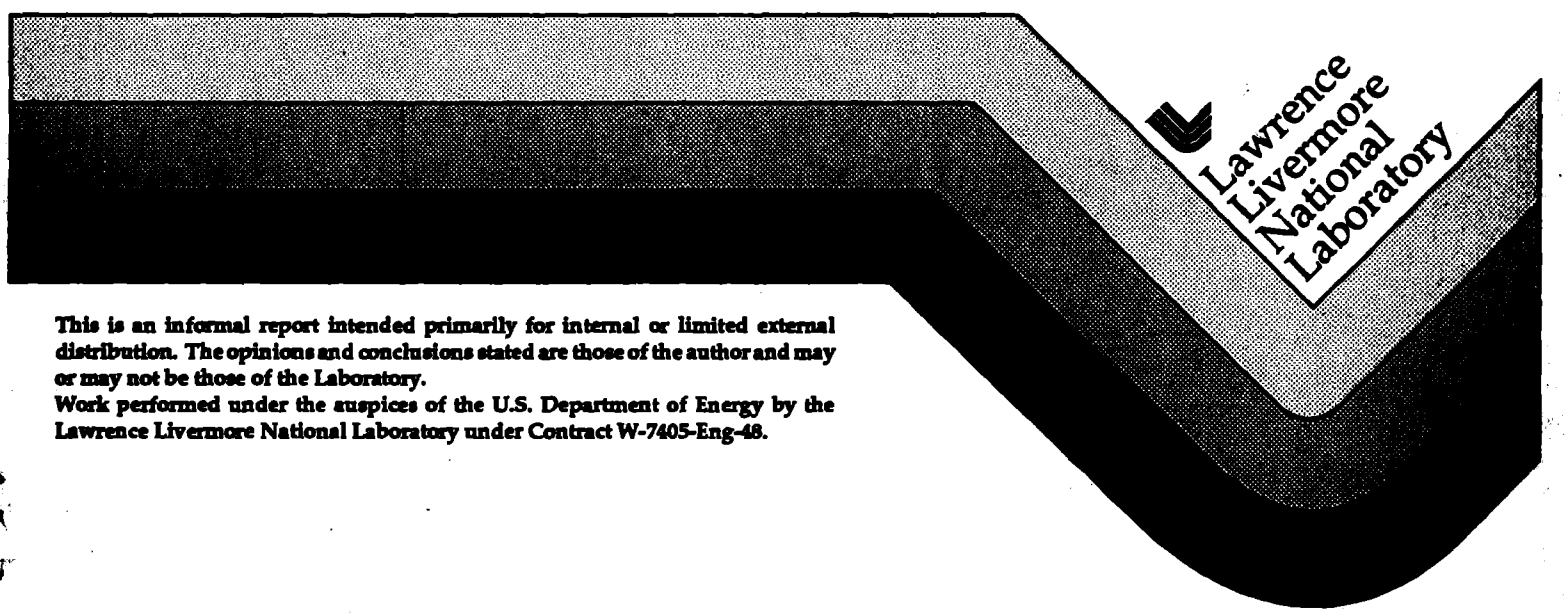

Work performed under the auspices of the U.S. Department of Energy by the Lawrence Livermore National Laboratory under Contract W-7405-Eng-48.

DISCLAIMER

Purpose for Handbook

This actuator and sensor handbook was developed during a cooperative project between the NASA-Marshall Space Flight Center, the SDI-Directed Energy Program and LLNL.

The common purpose of the joint effort was to develop precision actuators and sensors for the NASA initiated SpacE Laser ENErgy Program (SELENE). The purpose of the SELENE Program is to develop a highly cost effective segmented adaptive optics system for beaming laser power directly to spacecraft in earth orbit.

Acknowledgments

We wish to acknowledge the contributions of Dr. John D. G. Rather, NASA Headquarters, Dr. Edward E. Montgomery, Dr. James W. Bilbro, Dr. Steven C. Fawcett of NASA-Marshall Space Flight Center, George Sevaston of NASA-Jet Propulsion Laboratory, and Dr. Irving Stowers of Lawrence Livermore National Laboratory.

Table of Contents

List of Figures

List of Tables

Actuator Technologies

1. Linear Motion Hydraulic Actuator

Description of Actuator Technology

Typically, fluid systems are not considered for precision motion control; however, hydraulic systems can be designed such that they are nearly frictionless and exhibit no backlash. They are the only type of fluid system which can be employed for precision applications because gases are compressible. The operating principle is that the net force is the product of the fluid pressure and the surface area in contact with this pressure. Three general types of actuators exist which can achieve linear motion (Figure 1.1): cylinders, bellows, and the Poisson actuator.

A cylinder (Figure 1.1) consists of a moving rod attached to a piston which slides in and out of a cylinder. The motion is caused by fluid supplied to the cylinder. Fluid flow is typically controlled with servo valves. This type of actuator is well suited for large motion, moderate resolution motion. However, with the use of low friction seals and hydrostatic bearings to support the rod and cylinder, micrometer motion with high resolution can be achieved.[1]

A bellows configuration (Figure 1.2) consists of a deformable structure which replaces the need for the piston sliding in and out of a cylinder which requires a seal. This type of hydraulic actuator is typically used for small range of motion (up to 1 mm) precision positioning.

The Poisson actuator (Figure 1.3) is used when very small motion (< 3 μm) yet very large axial stiffness is desired. When a cylinder is internally pressurized, radial and axial strains occur which create radial and axial displacement. Pressure can be controlled either with a servo valve or by displacing a diaphragm with a second actuator.

Illustration of Actuator

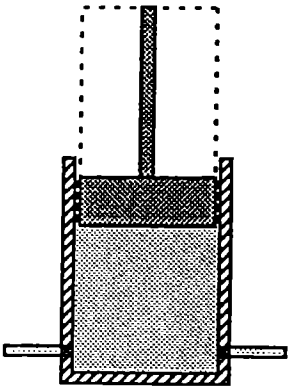

Figure 1.1 Single Action Piston Hydraulic Actuator

[1] Slocum, Alexander H., Massachusetts Institute of Technology. **Precision Machine Design.** Englewood Cliffs, NJ: Prentice Hall; 1992. 750 pages.

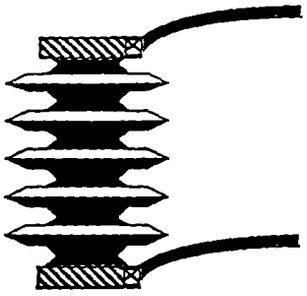

Figure 1.2 Hydraulic Bellows Actuator

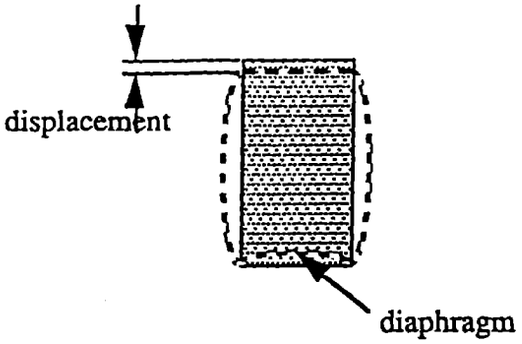

Figure 1.3 Poisson Actuator

Current Industrial Manufacturers

Air & Hydraulic Power, Inc.
Box 159T
555 Goffle Rd.
Wyckoff, NJ 07481
Telephone: (201) 447-1589
FAX: (201) 447-0302

ENERPAC
Dept. TR92
Butler, WI 53007
Telephone: (800) 433-2766
FAX: (414) 781-1049

Prince Mfg. Corp.
4600 Lewis Blvd.
Sioux City, IA 51102
Telephone: (712) 277-4061
FAX: (712) 277-8538

Current Availability

Large units available off-the-shelf. Small actuator with SELENE size and performance requirements will require custom design.

2. Electromagnetic Actuator

Description of Actuator Technology

A solenoid actuator (Figure 2.1) is comprised of a housing, moving rod, coils, and a spring. The moving rod is fabricated from a ferroelectric material which is surrounded by the coils. When a voltage is applied through the coils, a current flows through the coils which results in an electromagnetic force exerted on the moving rod, causing the rod to move. The movement of the rod caused by the electromagnetic force is always in a direction which tends to center the actuator in the magnetic field. A spring is typically used to counteract the electromagnetic force and return the moving rod to its initial position.[2] There is an inherent nonlinear relationship between the displacement and current input which exists for solenoids. Furthermore, because the actuator relies solely on the coil to create the magnetic circuit, the electromechanical time constant is relatively large. Because of these drawbacks, solenoids are typically used as inexpensive, non-precision actuators.

Voice coil actuators (Figure 2.2), or wound coil / permanent magnet actuators, avoid many of the problems associated with solenoids. Voice coils are commonly used in speakers. A permanent magnet is used to preload the electromagnetic circuit. The result is that small changes in current almost immediately cause a change in displacement. In effect, the permanent magnet increases the system bandwidth and linearizes system response.

Illustration of Actuator

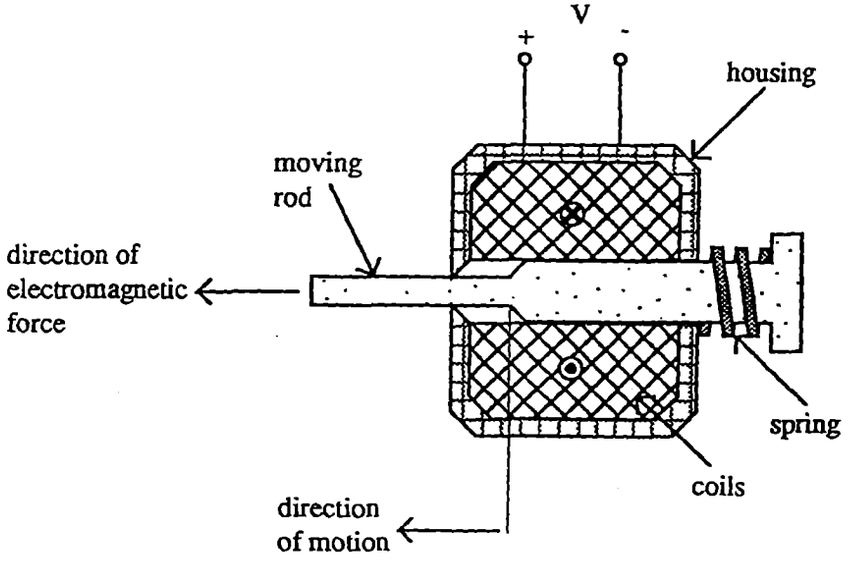

Figure 2.1 Solenoid

---

[2] Frangos, C.; Yavin, Y. **Current Controller Design for an Electromagnetic Actuator Using an On-Line Parameter Optimization Approach.** *IEEE Transactions on Industrial Electronics.* 1991 Feb; 38(1).

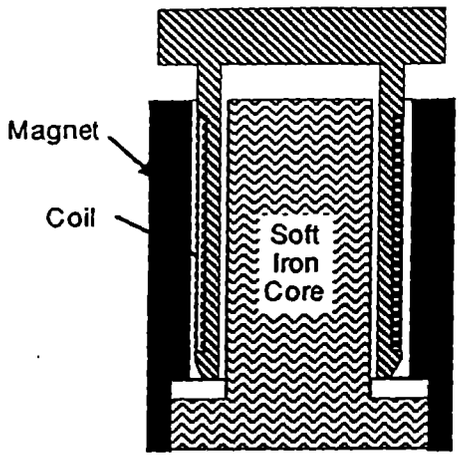

Figure 2.2 Voice Coil Actuator

Mathematical Model of Operating Principles

Solenoid

The force generated by a typical solenoid actuator is

$$F = \frac{N^2 I^2 A\mu}{2h^2} \tag{2.1}$$

where

N = number of turns in the coil,

I = current in the coil,

A = pole area,

μ = magnetic permeability of air (4π x 10^{-7} N / A^2), and

h = air gap.

Note the non-linear relationship between input current and output force.

Voice Coil

The relationship between mechanical force and current through a coil is

$$F = -Bli \tag{2.2}$$

where

B = flux density

l = length of the conductor, and

i = current through the coil.

The relationship expressing voltage as a function of velocity is

$$E = Bl\dot{x} \tag{2.3}$$

where

E = voltage.

Current Industrial Manufacturers

Northern Magnetics
16124 Wyandotte St.
Van Nuys, CA 91406
Telephone: (818) 997-8675
FAX: (415) 492-0231
Contact: Gary Burton @ (415) 492-0771 in San Rafael

Current Availability

Off-the-shelf components are available; however, they fail to meet SELENE specifications and are above cost requirements.

3. Electrostatic Actuator

Description of Actuator Technology

In an electrostatic actuator the driving force is generated by the repulsion or attraction of charges between parallel plates. Similar to potential energy in a capacitor, the electrostatic force is stored between the parallel plates for long periods of time; therefore, to return the plates to their original position, the electrical field between the plates must be removed. [3]

Illustration of Actuator

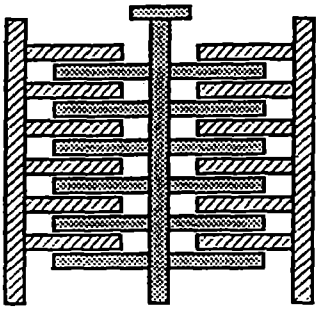

Figure 3.1 Electrostatic Actuator

Mathematical Model of Operating Principles[4]

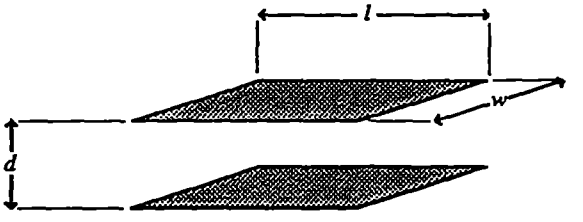

Figure 3.2 Parallel Plates

The capacitance between two plates (fingers) is

$$C = \varepsilon w \frac{l}{d} \tag{3.1}$$

where

C = capacitance

---

[3] Mason, P. M. **Electromechanical Transducers and Wave Filters.** Second ed. New York: D. Van Nostrand Company, Inc.; 1948: p. 187-215.

[4] Trimmer, W.; Gabriel, K. (AT&T Bell Laboratories Holmdel, NJ). **Design Considerations for a Practical Electrostatic Micro-Motor.** *Sensors and Actuators.* 1987; 11: p. 189 - 206.

ε = permittivity of medium between plates

w = plate width

l = plate length, and

d = separation distance between plates.

The potential energy is then

$$U = -\frac{1}{2}CV^2 \tag{3.2}$$

$$U = \frac{-\varepsilon\omega l V^2}{2d} \tag{3.3}$$

where

U = potential energy and

V = voltage applied across plates.

The force in a given direction can then be found by taking the partial derivative of the potential energy with respect to the direction of the force. The forces in each direction are

$$F_x = -\frac{\partial U}{\partial x} = \frac{\varepsilon l V^2}{2d} \tag{3.4}$$

$$F_l = -\frac{\partial U}{\partial l} = \frac{\varepsilon\omega V^2}{2d} \tag{3.5}$$

$$F_d = -\frac{\partial U}{\partial d} = -\frac{\varepsilon\omega l V^2}{2d^2} \tag{3.6}$$

where

F_x = force on the plates in the x direction

Fl = force on the plates in the l direction, and

F_d = force on the plates in the d direction.

The permittivity of air is 1.00134.

Current Availability

Not available as an off-the-shelf item. Requires custom design.

4. Ferroelectric Actuator

Description of Actuator Technology

Ferroelectricity is a phenomenon exhibited by certain polycrystalline ceramic materials (for instance lead zirconate titanate) in which an electrical field across the ferroelectric material creates deformation. When an electrical field is applied across two conductive plates with ferroelectric material between the plates, the ferroelectric mass extends in the direction of the electrical field and contracts in the direction normal to the electrical field.

Two actuator configurations have been developed. The bending configuration consists of two ferroelectric strips of material which are attached in opposing polarity. Consequently, when an electrical field is applied across the material, one strip increases in thickness and decreases in length while the second strip decreases in thickness and increases in length. The result is a bending motion which exhibits large displacements with relatively low forces. This configuration has a slow response rate and a low natural frequency.

The second configuration is composed of stacks of ferroelectric disks (Figure 4.2). When an electric field passes between the stack of disks, all material in the stack are exposed to equal stress. The result is a smaller displacement with large forces. In one typical stacked actuator, when an electrical field of 2000 V / mil is applied across the actuator, stresses between 34 to 45 MPa are achieved. It is necessary to axially preload the stack if bi-directional motion is desired because the stack is not reliable in tension. Ferroelectric actuators resemble capacitors in that when the electrical field is removed, the energy remains stored and the actuator remains in its displaced position.

In general, ferroelectric actuators exhibit fast response times and can produce large forces. However, a large hysteresis is an inherent feature of the ferroelectric material, as shown in the Figure 4.1.[5]

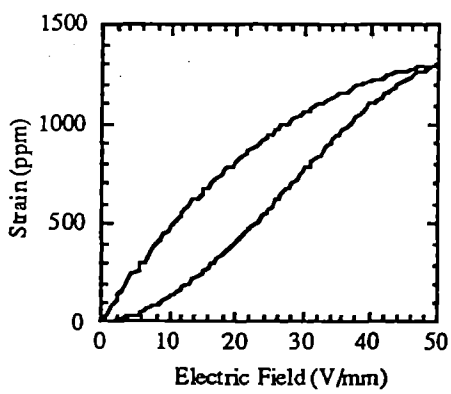

Figure 4.1 Hysteresis Effect

[5] O'Neil, C. G.; O'Neil, C. H. (Kinetic Systems, Hayword, CA). **Ferroelectric Actuators in the Electromechanical Interface.** *Optical Engineering.* 1990 Nov; 29(11): p. 1383-1388.

Illustration of Actuator

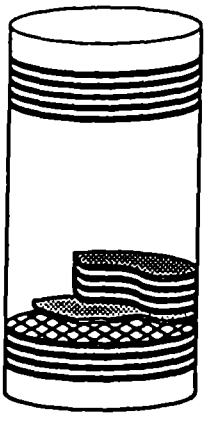

Figure 4.2 Ferroelectric Actuator

5. Electrostrictive Actuator

Description of Actuator Technology

Electrostriction is a phenomenon exhibited by all dielectric materials in which an electrical field produces physical deformation of the material. The amount of deformation is proportional to the square of the applied electrical field and therefore is independent of the direction of the electrical field (unlike piezoelectricity).[6] Total actuator strain is typically 500 ppm, or 0.5 μm / mm of actuator length.

Illustration of Actuator

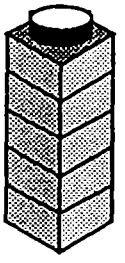

Figure 5.1 Lead Magnesium Niobate Actuator

Current Industrial Manufacturers

AVX Corp.
2875 Highway 501 West
Conway, SC 29526
Telephone: (803) 349-6264
Contact: Dr. Bharat Rawal

Litton / Itek Optical Systems
10 Maguire Rd.
Lexington, MA 02173
Telephone: (617) 276-2000
Contact: Mark Ealy

Current Availability

Available off-the-shelf. Frequency range is questionable with stacked units.

Current Pricing

Actuators used in a prototype SELENE configuration consisting of a few hundred actuators have been estimated to cost approximately $50 – $100 each. When production quantities go to hundreds of thousands, the cost per actuator could drop to under $10.

---

[6] Cady, W. G. **Piezoelectricity - An Introduction to the Theory and Applications of Electromechanical Phenomena in Crystals.** 2nd ed. United Kingdom: Dover Publications, Inc.; 1964; 1. 405 pages.

6. Piezoelectric Actuator

Description of Actuator Technology

Piezoelectricity is a phenomenon exhibited by certain crystal materials in which a mechanical strain on the material produces electrical polarization. The polarization is directly proportional to the applied strain. This is known as the direct piezoelectric effect. Piezoelectric actuators use the converse effect, in which strain is produced in a piezoelectric crystal when exposed to electrical polarization. This strain is directly proportional to the polarizing field and changes sign with the polarity of the field (unlike electrostriction).[7] The electrical field creates a torque on the aligned dipoles in the crystal structure which causes a length change. Lead-zirconium-titanate is commonly used as the piezoelectric crystal.[8]

The expansion of a piezoelectric material is not exactly proportional to the applied electrical field. This is illustrated in the hysteresis curve shown in Figure 6.1. The amount that a piezoelectric material expands or contracts is dependent on the voltage in which it was previously exposed to. The width of the hysteresis curve is as large as 15% of its covered path. In order to achieve absolute displacement with a piezoelectric actuator, a position controller with feedback from a position sensor is necessary.

Piezoelectric materials also exhibit drift. When the material changes shape, a slow drift in the same direction is observed. This is caused by continuing polarization of the ceramic crystals. In practice, the drift is only noticeable during the first few seconds after positioning. Again this can be controlled with the use of a position controller.

Piezoelectric expansion is also dependent on temperature. Like any material, piezolelectric materials have a coefficient of linear expansion which determines $\Delta L / L$. For typical stacked actuators, the thermal expansion coefficient (α) is:

$$\alpha = 11 \cdot 10^{-6} / °K \text{ (non-preloaded elements)}$$
$$\alpha = 7 \text{ to } 8 \cdot 10^{-6} / °K \text{ (preloaded elements)}$$

The piezoelectric effect is also temperature dependent. The expansion capacity of a piezoelectric material changes by approximately 0.2% / °K. Furthermore, above the Curie temperature of the material, polarization of the ceramic disappears, thus eliminating the piezoelectric effect. Temperatures

---

[7] Cady, W. G. **Piezoelectricity - An Introduction to the Theory and Applications of Electromechanical Phenomena in Crystals.** 2nd ed. United Kingdom: Dover Publications, Inc.; 1964; 405 pages.
[8] Physic Instrumente. **Products for Micropositioning.** US-edition ed. West Germany: p. 5.3-5.19.

above 300 °C cause complete depolarization. Temperatures around 150 °C begin to show irreversible depolarization. Therefore, this temperature should not be exceeded.

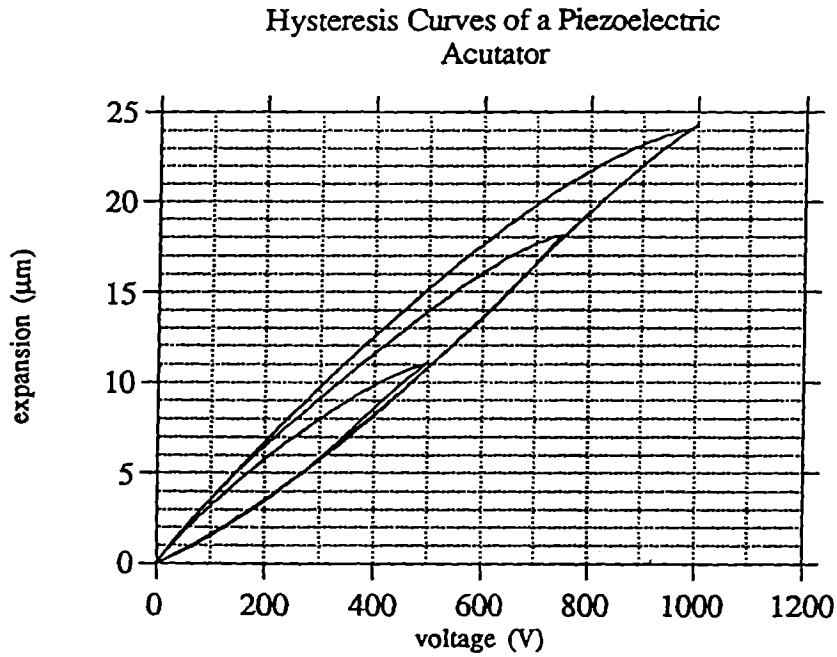

Figure 6.1 Piezoelectric Hysteresis

Illustration of Actuator

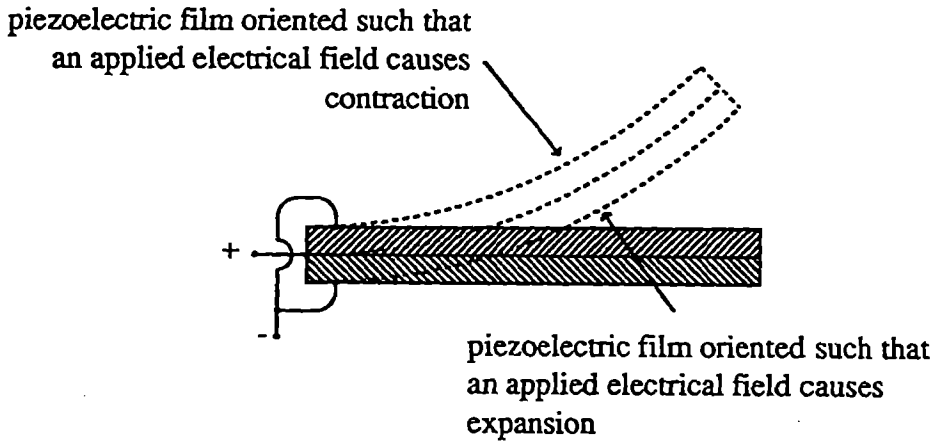

Figure 6.2 Bimorph

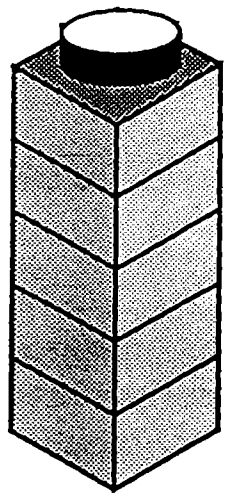

Figure 6.3 Stacked

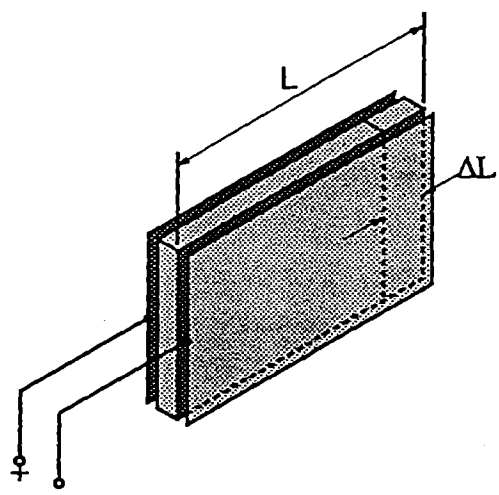

Figure 6.4 Laminar

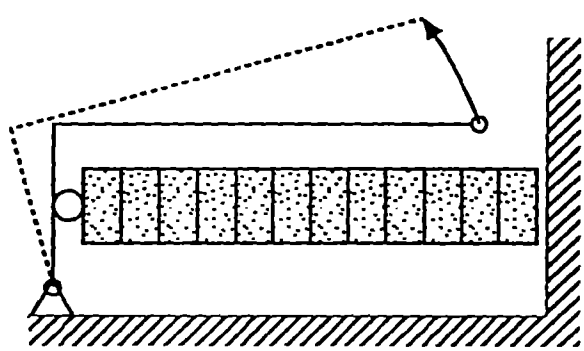

Figure 6.5 Hybrid

Mathematical Model of Operating Principles

Drift:

$$\Delta L(t) = \Delta L\left(1 + \gamma \cdot \ln\frac{t}{0.1}\right) \tag{6.1}$$

where

ΔL = the expansion 0.1 seconds after positioning (m)

γ = drift factor, which is dependent on the mechanical load and actuator configuration and lies between 0.01 and 0.02, and

t = time (s)

Strain:

The strain vector produced in a piezoelectric block by an external electrical field is

$$s = dE \tag{6.2}$$

where

s = strain vector

d = piezoelectric strain coefficient in tensor form, and

E = electric field.

The piezoelectric strain tensor coefficients, or the "*d*-constants", are the ratio of strain which develops along one axis to the electric field strength along the same or a different axis, assuming constant external stresses. The *d*-constant is expressed in terms if m / volt. To indicate axis, the *d*-constant is subscripted as d_{ij}, where i indicates the direction of the applied electric field and j indicates the direction of induced strain, For strain measured along the 3-axis (direction shown below)

$$s = d_{33}E \tag{6.3}$$

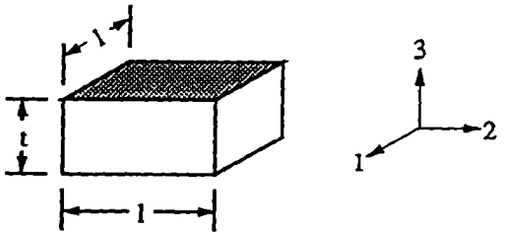

Figure 6.6 *Piezoelectric Cube Axis*

Substituting

$$s = \frac{\Delta t}{t} \tag{6.4}$$

and

$$E = \frac{V}{t} \tag{6.5}$$

into Eq. 6.3 reduces to

$$\Delta t = d_{33} V \tag{6.6}$$

where

Δt = change in length along the 3-axis (as illustrated above)

t = original length along the 3-axis, and

d_{33} = d-constant, ratio of strain along the 3-axis to the electrical field along the 3-axis.

For strains along the 1-axis or 2-axis, strain is

$$s = \frac{\Delta l}{l} = d_{31} \frac{V}{t} \tag{6.7}$$

where

Δl = change in length along the 3-axis (as illustrated above)

l = original length along the 3-axis, and

d_{31} = d-constant, ratio of strain along the 1-axis to the electrical field along the 3-axis.

Typical values of the d-constant are

d_{33} = 225 x 10^{-12} m / volt

d_{31} = -100 x 10^{-12} m / volt

for hard PZT, and

d_{33} = 600 x 10^{-12} m / volt

d_{31} = -275 x 10^{-12} m / volt

for soft PZT.

Compliance:

A stress-strain curve can be generated by applying a voltage which creates a given strain (0 stress), and then adding a load which returns the material to its original dimensions (0 strain). Curves can be generated for various input voltages. The slope of the stress-strain curve is the compliance of the piezoelectric material. The compliance in the 3-direction is

$$\frac{\Delta t}{t} = S_{33}{}^{E} \frac{F_3}{l^2} \tag{6.8}$$

where

$S_{33}{}^{E}$ = elastic compliance [m^2 / N] (strain in the 3-direction due to stress in the 3-direction)

F_3 = uniaxial force in the 3-direction [N], and

l^2 = area on top of the piezoelectric block.

The E superscript on the elastic compliance indicates that the compliance is measured under "short circuit" conditions where a constant charge is maintained on the electrodes. A corresponding **D** superscript indicates an "open circuit" condition. The corresponding equation for compliance in the 1-direction is

$$\frac{\Delta l}{l} = S_{11}{}^{E} \frac{F_1}{lt}, \tag{6.9}$$

where

$S_{11}{}^{E}$ = elastic compliance [m^2 / N] (strain in the 1-direction due to stress in the 1-direction)

F_1 = uniaxial force in the 1-direction [N], and

lt = area on the side of the piezoelectric block.

Typical values of the elastic compliance are

$$S_{33}{}^{E} = 20 \times 10^{-12}\ m^2 / N$$
$$S_{31}{}^{E} = 15 \times 10^{-12}\ m^2 / N$$

for hard PZT, and

$$S_{33}{}^{E} = 15 \times 10^{-12}\ m^2 / N$$
$$S_{31}{}^{E} = 12 \times 10^{-12}\ m^2 / N$$

for soft PZT.

Expansion equations:

$$\Delta L = E \cdot d \cdot L_o + \frac{F}{c_T} = \Delta L_o + \frac{F}{c_T} \tag{6.10}$$

where

DL = change in length (m)

E = electric field strength (V / m)

d = direction dependent material constant (or piezoelectric strain constant), which is a function of both the material and the field strength

L_o = length of material with no field present (m)

F = preload force (N)

c_T = material stiffness, and

ΔL_o = nominal expansion without applied force (m).

Maximum expansion is limited by the maximum electric field strength without causing damage by voltage sparkovers. Maximum electrical field lies in the range of 1 to 2 kV / mm. With a d_{33} of 225 x 10^{-6} µm / V leads to a strain of 450 ppm.

Maximum force:

When the piezoelectric material is placed between infinitely stiff walls, the maximum force is

$$F_{\max} = c_T \cdot \Delta L_o \tag{6.11}$$

However, in reality the force is smaller than this because the mounting material will not have infinite stiffness. The maximum effective force now becomes

$$F_{eff} = c_T \cdot \Delta L_o \left(1 - \frac{c_T}{c_T + c_S}\right) \tag{6.12}$$

where

F_{eff} = maximum effective force, and

c_S = stiffness of mounting material.

Resonant frequency:

The resonant frequency of any system is dependent on its mass and elastic properties. The resonant frequency of the actuator is also dependent on any mass attached to the actuator. The mass which the actuator is moving will reduce the resonant frequency. Resonant frequency of the piezoelectric material itself is

$$f_o = \frac{1}{2\pi}\sqrt{\frac{c_T}{m_{eff}}} \tag{6.13}$$

where

f_o = resonant frequency (Hz), and

m_{eff} = effective mass, which is m / 2 when one end is fixed.

When a mass is attached to the actuator,

$$f_o' = f_o\sqrt{\frac{m}{m+2M}} \tag{6.14}$$

where

f_o' = resonant frequency (Hz) with additional mass, and

M = attached mass.

Time requirements for expansion:

The time requirement for a piezoelectric material to reach its nominal expansion is approximately 1 / 3 the effective resonant frequency. It should be noted that an additional mass attached to the actuator reduces the resonant frequency and thereby also increases the expansion time. The minimum expansion time of a piezoelectric material is

$$T_{\min} \approx \frac{1}{3 \cdot f_o'} \tag{6.15}$$

where

T_{min} = shortest expansion time.

Dynamic forces:

A force is generated in a piezoelectric material when an extremely fast voltage change occurs. (This force can be a pushing or pulling force. However, to achieve a tensile force the material must be preloaded to prevent the ceramic stack from exceeding its fracture strength.) This force is

$$F = c_T \cdot \Delta L = \pm 4\Pi^2 \cdot m_{eff} \cdot \Delta L \cdot (f_o')^2 \tag{6.16}$$

where

F = preload force (N)

c_T = material stiffness

ΔL = change in length (m)

m_{eff} = effective mass, which is m / 2 when one end is fixed, and

f_o' = resonant frequency (Hz) with additional mass.

When the motion is sinusoidal, the maximum dynamic force is

$$F_{dyn} = \pm 4\Pi^2 \cdot m_{eff} \cdot \frac{\Delta L}{2} \cdot f^2 \tag{6.17}$$

where

F_{dyn} = maximum dynamic force (N), and

f = frequency of sinusoidal motion.

Quasi-static control:

When a piezoelectric material expands, a change in its charge occurs, resulting in the current

$$i = \frac{dQ}{dt} = C \cdot \frac{dU}{dt} \tag{6.18}$$

where

i = current (A)

Q = charge (C)

t = time (s)

C = capacitance (F), and

U = operating voltage (V).

For quasi-static motion, a small, low-power high voltage supply can be used as the driver.

Dynamic control:

The frequency at which position can be controlled is limited by the resonant frequency. The resonant frequency decreases when additional mass is attached to the actuator. A safe estimate is that dynamic control can be achieved to approximately 80% of the resonant frequency.

The maximum frequency at which the actuator can be controlled is also dependent on the peak current which can be supplied by the amplifier (which should be given in the technical data of the amplifier). The frequency limit can be estimated by

$$f_{\max} = \frac{i_{\max}}{2 \cdot C \cdot U_o} \tag{6.19}$$

where

f_{max} = maximum frequency (Hz)

i_{max} = peak current supplied by amplifier, and

U_o = nominal operating voltage.

Furthermore, the charging time of the actuator under constant current is

$$t = C \cdot \frac{U_o}{i_{\max}} \tag{6.20}$$

where

t = charging time (s).

Power requirements:

The power requirement of the amplifier is

$$P_{out} = C \cdot U \cdot U_o \cdot f \tag{6.21}$$

where

P_{out} = power requirement (W)

C = capacitance of piezoelectric material (F)

U = operating voltage (V)

U_o = maximum output voltage, and

f = operating frequency.

Heating:

When a piezoelectric material is charged, the energy stored is

$$E = \frac{1}{2} C U^2 \tag{6.22}$$

where

E = stored energy (J)

C = capacitance of piezoelectric material (F), and

U = operating voltage (V).

Most of the energy flows back to the power supply during discharge. About 5-8% of the energy is converted into heat. The energy efficiency is represented by the electromechanical coupling factor,

$$k = \sqrt{\frac{E_m}{E_e}} \tag{6.23}$$

and is usually expressed as a percent. The electromechanical coupling factor is generally expressed with two subscripts. The first subscript indicates the direction of electrical field and the second subscript indicates the direction of mechanical strain. For most applications the important coefficients are k_{33} and k_{31}. For quasi-static motion, the heat can be ignored. However, for dynamic operations with large amplitudes exceeding 100 Hz, the actuator will heat up. Frequencies higher than 100 Hz require cooling. The thermal heat which is generated is

$$P \approx \tan\delta \cdot f \cdot C \cdot U^2 \tag{6.24}$$

where

P = thermal heat (J)

$\tan\delta$ = angle of loss (approximately 0.05), and

f = operating frequency.

Electrical substitute circuit diagram:

A piezoelectric actuator is a spring mass system and can be represented by the following circuit diagram.

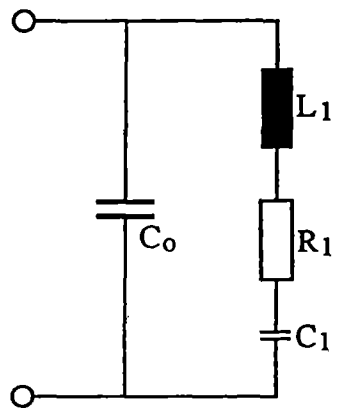

Figure 6.7 Piezoelectric Equivalent Circuit

For quasi-static motion, only the main capacitance C_0 appears. For higher frequency operations, the serial resonance circuit connected in parallel with C_0 must be considered.

Current Industrial Manufacturers

Physik Instrumente (PI)
GmbH & Co.
Siemensstrasse 13-15
W-7517 Waldbronn
Germany
Telephone: 49-72-436040
FAX: 49-72-4360445
Telex: 78-2859

In USA
Polytec Optronics Inc.
3001 Redhill Ave.
Bldg. 5, Suite 102
Costa Mesa, CA 92626
Telephone: (714) 850-1835

Burleigh Instruments, Inc.
Burleigh Park
Fischer, NY 14453
Telephone: (716) 924-9355
FAX: (716) 924-9072
Telex: 97-8379

Morgan Matroc, Inc.
Vernitron Division
232 Forbes Road
Bedford, OH 44146
Telephone: (216) 232-8600
FAX: (216) 232-8731
Contact: George Glazner

Current Availability

Available off-the-shelf.

Current Pricing

Stacked actuator, up to 80 μm expansion - $1755 (PI)
Stacked actuator, up to 40 μm expansion - $970 (Burleigh)
Three actuator tilting unit, 10 μm expansion and 1 mrad tilt - $3390 (PI)
Three actuator tilting unit, 6 μm expansion and 75 arcsec tilt - $1020 (Burleigh)

7. Inchworm-type Piezoelectric Actuator

Description of Actuator Technology

One inchworm-type actuator utilizes a dual positioning system, where a friction drive and a piezoelectric actuator move together in an inchworm-type movement. The friction drive is used for course positioning and provides a large stroke. The piezoelectric actuator is used for fine positioning, providing high resolution. As the two actuators move together, attributes of both technologies are combined.

During the inchworm-type movement, the piezoelectric actuator expands to a predetermined length. When this length is achieved, the friction drive extends the actuator further. Simultaneously, the piezoelectric actuator contracts to the original length and then again expands. This procedure is repeated, thus achieving the inchworm-type movement.[9]

Inchworm-type movement can also be achieved without the use of a friction drive motor. This is accomplished by an active clamping mechanism which holds one end of the piezoelectric expander in place. The opposite end is free, and in the presence of an electrical field, this end expands. The free end is then actively clamped and the originally fixed end is freed. The electrical field is removed and the free end now contracts. Once again the clamped end is freed and the free end is clamped. This process is repeated to achieve an inchworm-type motion. Advantage to this method is an increased stroke.

An inertial recoil displacement device can also create inchworm-type motion. Again, one end of the piezoelectric actuator is actively clamped. The free end is attached to an acceleration mass. First, an electrical field is applied which causes the free end to expand. As the free end expands, the acceleration mass is moved, and thus the center of gravity is shifted in the direction of movement. Next, the clamped end is released and the electrical field is removed. Because the center of mass has changed, the ends of the piezoelectric element move toward the new center of mass. This process is repeated to achieve an inchworm-type motion.[10]

---

[9] Sakuta, S.; Ueda, K.; Ogawa, K.; Moriwaki, Y.; Sumiya, Mitsuo (Toshiba Corp, Yokohama, Jpn). **Precision Dual Positioning System.** *Proceedings of SPIE - The International Society for Optical Engineering*; 1990 Jul 9; San Diego, CA. Bellingham, WA: Int Soc for Optical Engineering; 1990; 334: p. 10-17.

[10] Robbins, W. P.; Polla, D. L.; Glumac, D. E. **High-Displacement Piezoelectric Actuator Utilizing a Meander-Line Geometry -- Part I: Experimental Characterization.** *IEEE Transactions on Ultrasonics, Ferroelectrics, and Frequency Control.* 1991 Sep; 38(5).

Illustration of Actuator

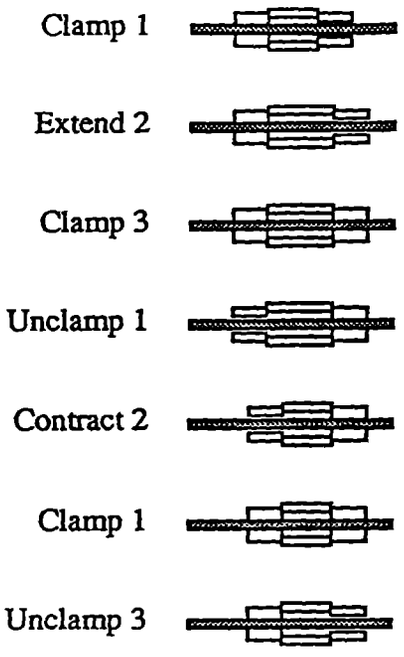

Figure 7.1 Inchworm-type Piezoelectric Actuator

Current Industrial Manufacturers

Burleigh Instruments, Inc. (have patent on inchworm design)
Burleigh Park
Fishers, NY14453
Telephone: (716) 924-9355
FAX: (716) 924-9072
Telex: 97-8379

Current Availability

Available off-the-shelf.

8. Shape Memory Alloy Actuator

Description of Actuator Technology

Shape memory alloys are metal alloys such as nickel titanium (nitinol) which, when deformed and then exposed to an elevated temperature, return to their original undeformed shape. When the shape memory alloy is heated to a specific transition temperature, easily deformable martensite structures experiences a phase transition and transforms into a rigid crystalline austenite structure. During this transformation, the material attempts to return to its original shape. SMA's can be configured in the form of sheets, wires, foils, or thin films. They require large amounts of power, to cause the phase transformation and consequently are very low efficiency actuators.[11]

Illustration of Actuator

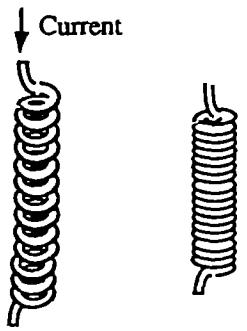

Figure 8.1 Shape Memory Alloy Actuator

Current Industrial Manufacturers

TiNi Alloy Co.
Oakland, CA
Telephone: (510) 483-9676

Dynalloy, Inc.
Irvine, CA
Telephone: (714) 476-1206

Current Availability

Material available off-the-shelf. Actuator requires custom design.

Current Pricing

~ $5 – $10 / meter

---

[11] Studt, T., Senior Editor (R&D Magazine). **Smart Materials: Creating Systems That React.** *R&D Magazine.* 1992 Apr; : p. 54-60.

9. Thermomagnetic Actuator

Description of Actuator Technology

A thermomagnetic material is a magnetic material with a low Curie point in which the magnetic strength is a function of the temperature. A thermomagnetic actuator is comprised of a temperature-sensitive magnet, a moving rod, and excitation coils for control. The displacement of the moving rod is dependent on both the excitation in the coils and the temperature. The coils can be replaced by a permanent magnet, thus eliminating the need for external power. The thermomagnetic material can also serve as a temperature sensor. This type of actuator achieves excellent output characteristics with large displacements.[12] [13]

Illustration of Actuator

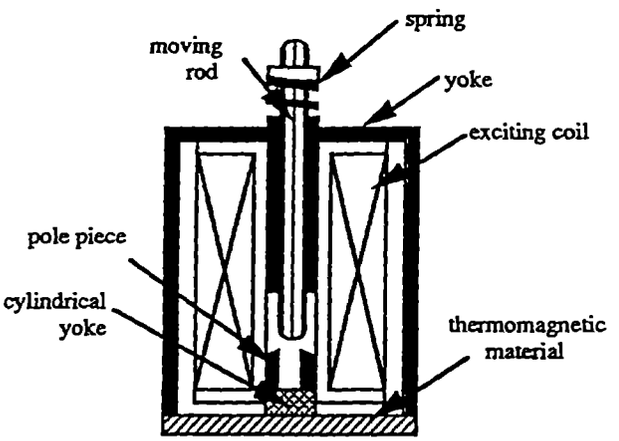

Figure 9.1 Thermomagnetic Actuator

Current Industrial Manufacturers

None.

Current Availability

Requires custom design.

---

[12] Yamasawa, K. (Member, IEEE). Performance of Temperature-Sensitive Magnetic Actuators. *IEEE Transactions on Magnetics*. 1985 Nov; vol mag-21(no 6): p. 2652-2656.

[13] Yamasawa, K.; Biringer, P. (Member, IEEE). **Graphical Analysis of Thermomagnetic Actuator with Hybrid Excitation.** *IEEE Transactions on Magnetics*. 1990 Nov; vol 26, no 6: p. 3124-3128.

10. Magnetostrictive Actuator

Description of Actuator Technology:

A magnetostrictive material changes shape when exposed to a magnetic field. This phenomenon is known as the Weidemann effect. The magnetostrictive expansion can be used to create linear motion with high forces and very fast response times. Actuators made from magnetostrictive materials are efficient, operate at low voltage, and transmit large amounts of energy per volume. In the past, magnetostrictive materials were not considered for actuators because they produced significantly less strain than piezoelectric and electrostrictive materials. However, recently a new magnetostrictive material, ETREMA Terfenol-D®, offers strains 40 times greater than the original magnetostrictive materials, and performs an order of magnitude better than piezoelectric materials. ETREMA Terfenol-D® is an alloy of terbium, dysprosium, and iron (typically $Tb_{0.3}Dy_{0.7}Fe_{1.95}$).

Linear motion is achieved by exciting a magnetostrictive rod with a magnetic field. The magnetic field is produced by surrounding the rod with a coil and passing a current through the coil. End caps made of high-permeability iron reduce fringing of the magnetic field at the end of the rod. If it is necessary for the rest position to be in the center of the rod motion, biasing may be necessary. Biasing can be achieved by adding a permanent magnet to the magnetic circuit. A biased actuator will extend for the first half of the cycle and contract for the second half of the cycle.

Most actuators are designed to provide strains of around 1000 ppm, although strains as large as 2000 ppm are achievable. Within this range, displacement is linearly proportional to the input current; however, some hysteresis does occur. Typically, a 0.25 inch diameter rod can produce 50-75 lb, while a 2 inch diameter rod can produce forces over 1000 lb. Actuator response time is only limited by the time required to generate the coil current (as short as 10 μs). ETREMA Terfenol-D® does not fatigue. Furthermore, little heat is generated during cycling of the material.

A second material which exhibits magnetostrictive properties is Permendur, and alloy comprised of 49% Fe, 49% Co, and 2% V[14]. This material has been used for a high-precision spring type displacement transducer. The spring-type magnetostriction actuator (STMA) can achieve displacements of 50-100 μm with an accuracy of 0.1 μm in 1-10 ms. Resonant frequencies of approximately 600 Hz open loop were observed. The STMA has been developed and tested in two different optomechanical devices at the Academy of Sciences in Moscow. In these devices, a closed loop design was chosen to create a linear response with no hysteresis. Feedback made use of the inverse Weidemann effect, where a displacement causes a change in the magnetic field, which can be

---

[14] Aksinin, V.; Apollonov, V.; Borodin, V.; Brynskikh, A.; Chetkin, S.; Murav'ev, S.; Ostanin, V.; Vdovin, G. (General Physics Institute, Academy of Sciences, Moscow). **Spring-type Magnetostriction Actuator Based on the Wiedemann Effect.** *Sensors and Actuators.* 1990; A21-A23: 236-242.

determined by measuring the voltage through the coil. Repeatability and linearity of 0.1% of full scale were achieved by using the inverse Weidemann effect.

The following table summarizes the material properties.

Table 1 ETREMA Terfenol-D® Material Properties

MECHANICAL	
Density	9.25 x 10^3 kg / m^3
Bulk Elastic Modulus	9.0 x 10^{10} N / m^2
Young's Modulus	2.5 - 3.5 x 10^{10} N / m^2
Tensile Strength	28 MPa
Compression Strength	700 MPa
THERMAL	
Expansion Coefficient	12 x 10^{-6} / °C
Specific Heat Capacity	0.32 - 0.37 J / g / °K
Thermal Diffusivity	0.035 - 0.03 cm^2 / s
Thermal Conductivity	10.5 - 10.8 J / °C / m / s
ELECTRICAL	
Resistivity`	60 μΩ cm
MAGNETIC	
Magnetization	1.0 T
Curie Temperature	380 °C
MAGNETOSTRICTIVE	
Magnetostriction	1500 - 2000 ppm
Energy Density	1.4 - 2.5 x 10^4 J / m^3
MAGNETOMECHANICAL	
Relative Permeability	5 - 10
Coupling Factor	0.7 - 0.75
Sound Speed	1720 m / s

Illustration of Actuator

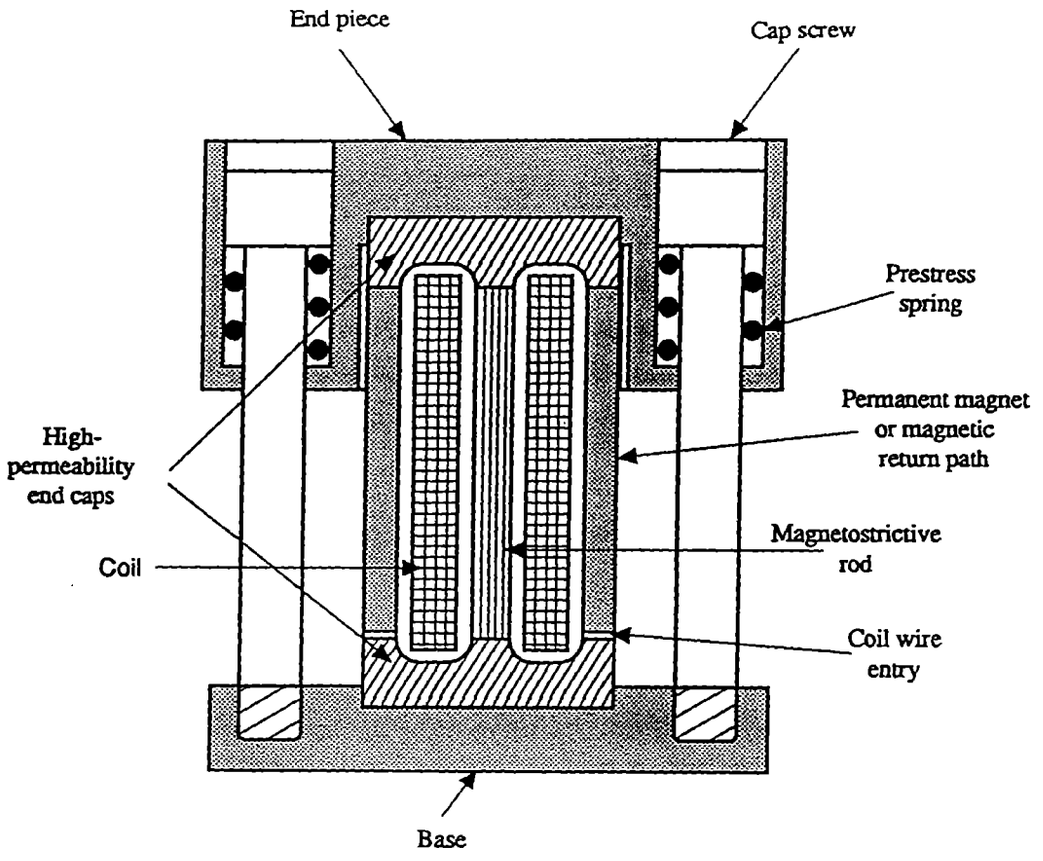

Figure 10.1 Magnetostrictive Actuator

Mathematical Model of Operating Principles

The force generated by the magnetostrictive rod is

$$F = EA\Delta L / L \tag{10.1}$$

where

E = Young's modulus (see table)

A = cross-sectional diameter of rod

F = force generated by rod

ΔL = change in length of rod, and

L = original length of rod.

A magnetic field is produced by current flowing through a coil. The strain produced by this magnetic field can be determined by

$$S = s^H T + dH \tag{10.2}$$

$$S = \frac{\Delta L}{L} \tag{10.3}$$

where

S = strain [dimensionless]

s^H = open circuit inverse Young's modules

T = mechanical stress

d = magnetostrictive "d" constant

H = magnetic field intensity

ΔL = change in length due to Weidemann effect

L = original length of magnetostrictive material

and

$$s^H = \frac{1}{Y^H} \tag{10.4}$$

where

Y^H = nominal open circuit Young's modulus.

The "d" constant corresponds to the slope of the S-H curve (shown below) in the intended operation region.

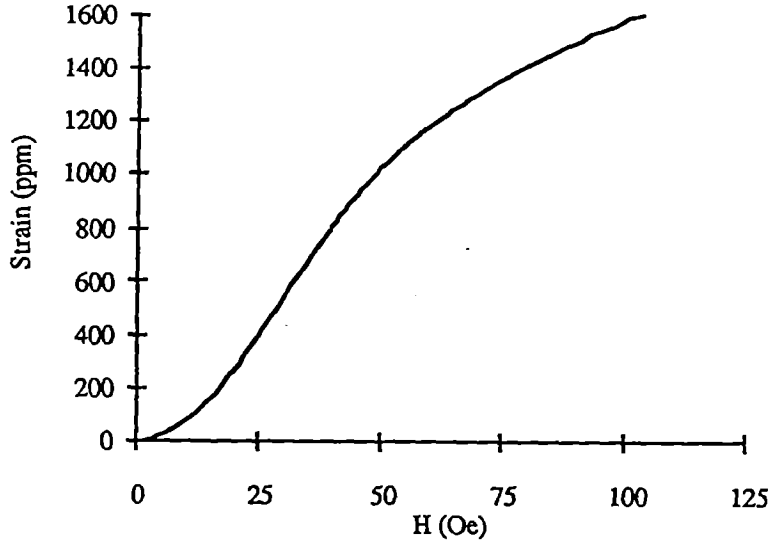

Figure 10.2 Strain vs. Magnetic Field Intensity [15]

[15] Butler, Dr John L., Image Acoustics, Inc., N. Marshfield, MA. **Application Manual for the Design of ETREMA Terfenol-D® Magnetostrictive Transducers.** Ames, Iowa: ETREMA Products, Inc., Subsidiary of EDGE Technologies, Inc.; 1988. 59 pages.

In the linear operating region, the "d" constant is approximately 1.6 x 10^{-6} Oe^{-1}, or 20 x 10^{-9} m / A. The "d" constant in the linear region can also be calculated by

$$d = k\sqrt{\frac{\mu^T}{Y^H}} \tag{10.5}$$

where

μ^T = free permeability (11.56 x 10^{-6} H / m for ETREMA Terfenol-D®), and

k = coupling coefficient (0.72 for ETREMA Terfenol-D®).

The coupling coefficient is the square of the ratio of converted energy to stored energy, and is thus an indication as to the efficiency of the material. For ETREMA Terfenol-D®, a coupling coefficient of 0.72 is equivalent to 51.8% of the energy being converted to mechanical energy.

The magnetic field intensity created by flowing current through a coil can be determined by

$$H = nI \tag{10.6}$$

where

n = turns in coil per unit length, and

I = current through coil.

There is a maximum amount of energy which can be transferred to mechanical energy, corresponding to a saturation point. This can be found by

$$E_m = \frac{\mu^T (kH_{max})^2}{2}. \tag{10.7}$$

For ETREMA Terfenol-D® material, this occurs at approximately 1000 Oe and 1400 ppm strain. Higher strains for a given applied field can be achieved by prestressing the material. At a strain of 1000 ppm, the following table illustrates the required magnetic field.

Table 2 Compressed ETREMA Terfenol-D® Magnetic Field

Pressure (MPa)	Pressure (k psi)	≈H (kA / m) @ 1000 ppm strain
6.9	1.0	50
9.6	1.4	40
12.4	1.8	45
15.1	2.2	40
17.9	2.6	55
20.7	3.0	60
24.1	3.5	75

The operating frequency is limited by eddy currents which flow through the rod. The cutoff frequency is

$$f_c = \frac{2\rho_e}{\pi\mu_s D^2} \tag{10.8}$$

where

f_c = cutoff frequency (Hz)

ρ_e = resistivity of magnetostrictive material

D = diameter of magnetostrictive rod, and

$$\mu_s = \mu_T\left(1-k^2\right) \tag{10.9}$$

where again

μ^T = free permeability (11.56 x 10^{-6} H / m for ETREMA Terfenol-D®), and

k = coupling coefficient.

The inductance of the magnetostrictive rod can be calculated with the equation

$$L = \mu^T N^2 \frac{A}{L} \tag{10.10}$$

where

L = inductance [H]

μ^T = free permeability

N = number of turns in the coil (= nL)

A = area of magnetostrictive rod, and

L = length of magnetostrictive rod.

Current Industrial Manufacturers

ETREMA Products, Inc.
A Subsidiary of EDGE Technologies, Inc.
306 South 16th
Ames, IA 50010
Telephone: (515) 232-0820
(800) 327-7291 USA Only
FAX: (515) 232-1177
Contact: Mel Goodfriend or Larry Voelker

Current Availability

Actuator units available off-the-shelf in a limited number. Most likely requires custom design. Material Terfenol-D may also be purchased off-the-shelf.

Current Pricing

For a few hundred actuators, cost is approximately $250 / actuator plus engineering costs. For hundreds of thousands of actuators price goes to $100 - $125 / actuator.

Table 3 Actuator Technologies

	Resolution [μm]	Range [μm]	Linearity [% F.S.]	Hysteresis [% F.S.]	Bandwidth [kHz]
Hydraulic	—	—	—	—	—
Electromagnetic	—	—	—	—	—
Electrostatic	—	—	—	—	—
Ferroelectric[16]	5×10^{-3} (typ)	40 (typ)[17]	$1^1/_2$%	3% -30%	16-18 kHz[18]
Electrostrictive	—	—	—	—	—
Piezoelectric*	0.002- 0.004	5-180(S) 50-1000(H) 20-45(L) 100(B) 6,250- 200,000(I)	1% (soft) 2%-10% (hard)	2%-20%	2-70(S) 0.1-2.2(H) 8.3-13(L) 2.5(B)
SMA	—	—	—	—	—
Thermomagnetic	—	—	—	—	—
Magnetostrictive	—	ΔL/L=1000-2000	—	—	150-2000 Hz

* (S) = stacked configuration; (H) = hybrid configuration, (L) = laminar configuration; (B) = bimorph configuration;

(I) = inchworm configuration

[16] O'Neil, C. G.; O'Neil, C. H. (Kinetic Systems, Hayword, CA). **Ferroelectric Actuators in the Electromechanical Interface.** *Optical Engineering*. 1990 Nov; 29(11): p. 1383-1388.

[17] Range for 127 stacks. Range increases with number of stacks.

[18] Frequency for a 1 inch stack. As stack increases, mass increases and natural frequency is reduced.

Edge Sensor Technologies

11. Optical Heterodyne Interferometry

Description of Sensor Technology

Optical heterodyne interferometry measures changes in distance by creating interference between two beams, similar to the Michelson interferometer. Ring-shaped interference patterns are produced in the image plane of the source and measured to determine distance changes between the test surface and reference surface.

Light from a single laser source is split into two beams of different frequency and polarization. A reference phase is obtained by mixing the two beams before they are sent to the interferometer. The phase or frequency of the signal obtained by the interfering beams is compared to this reference frequency to directly determine distance.[19]

Illustration of Sensor

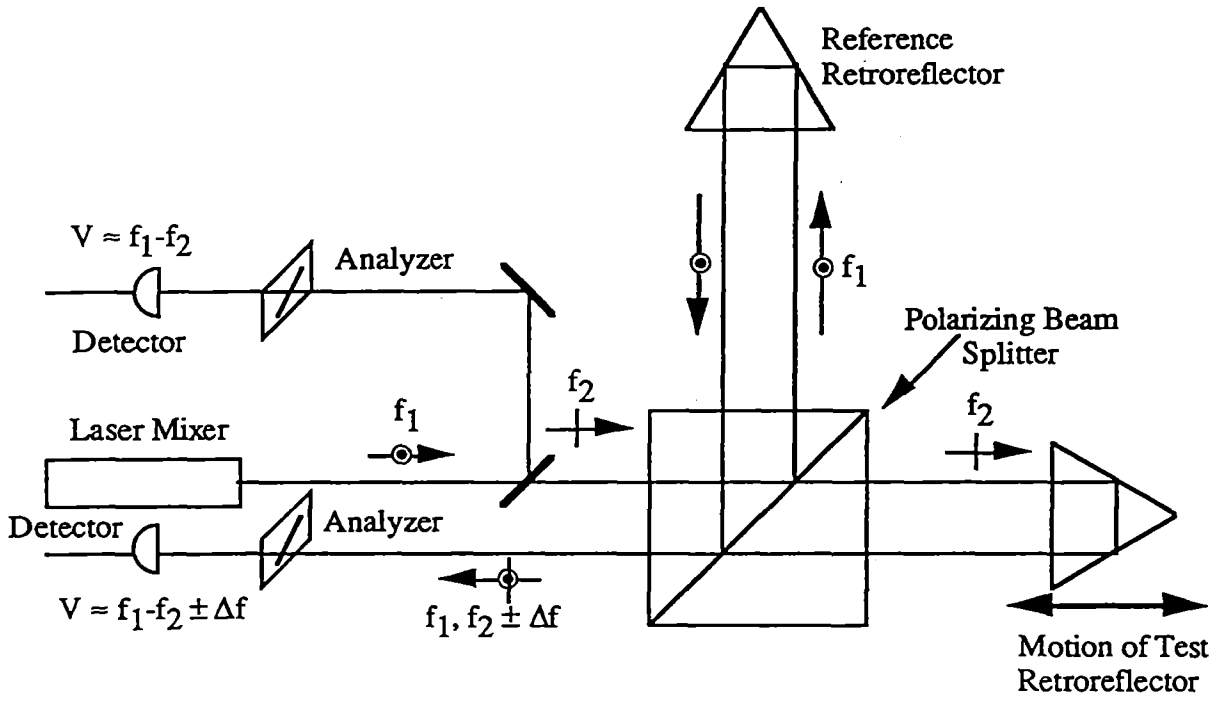

Figure 11.1 Optical Heterodyne Interferometry

Mathematical Model of Operating Principles

The reference detector signal is

---

[19] Teague, C. T. (National Institute of Standards and Technology). **AIP Conference Proceedings 241 Scanned Probe Microscopy.** Wickramasinghe, H. K. *Nanometrology*; 1991; Santa Barbara, CA. ; 1991. 371-407 pages.

$$V_R = \cos[2\pi(f1 - f2)t] \tag{11.1}$$

where

$f1$ = frequency of one beam split from the source, and

$f2$ = frequency of second beam split from the source.

The detector signal at the measurement detector is

$$V_m = \cos[2\pi(f1 - f2)t + \phi] \tag{11.2}$$

where

ϕ = time varying phase shift caused by motion between the measurement arm and reference retro-reflector arm (see figure).

The distance between the reference arm and the measurement arm can be determined directly from the phase difference between V_m and V_R. They are related by

$$\frac{\phi}{2\pi} = \frac{2\mu L}{\lambda_o} \tag{11.3}$$

where

λ_o = wavelength of radiation in a vacuum

L = effective separation between test and reference surfaces, and

μ = refractive index of the medium in the optical paths.

Current Industrial Manufacturers

Zygo Corp.

Hewlett Packard

Current Availability

Not available in configuration appropriate for SELENE edge sensors. Invention necessary.

12. X-Ray Interferometry And Optical Scales

Description of Sensor Technology

Both the X-ray interferometer and optical scales uses the diffraction grating interferometer configuration shown below. Three gratings are used: (1) a splitter grating S, (2) a mirror grating M, and (3) an analyzer grating A. The splitter grating separates the incoming light into two coherent beams which travel different paths. The mirror grating then brings the two split beams back into coincidence at the analyzer grating. Diffraction patterns are created at the analyzer grating by the recombining beams. As the analyzer grating is displaced in the indicated direction, intensity changes occur between A and B beams, varying sinusoidally with the periodicity of the diffraction gratings and independent of the wavelength of light. For x-ray interferometry, the model is altered to include the theory of x-ray diffraction.[20]

Illustration of Sensor

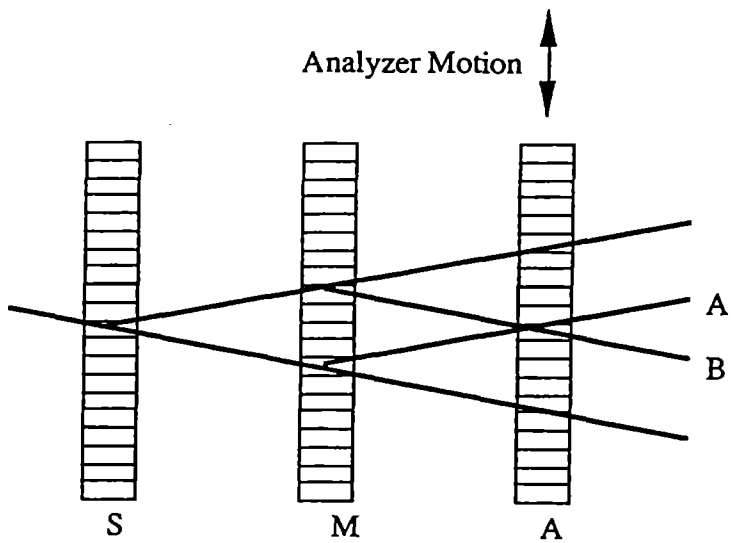

Figure 12.1 Diffraction Grating Interferometer

Current Availability

Not available in configuration appropriate for SELENE edge sensors. Invention necessary.

[20] Teague, C. T. (National Institute of Standards and Technology). **AIP Conference Proceedings 241 Scanned Probe Microscopy.** Wickramasinghe, H. K. *Nanometrology*; 1991; Santa Barbara, CA. ; 1991. 371-407 pages.

13. Inductive (Eddy Current) Transducer

Description of Sensor Technology

An inductive proximity probe is a cylindrical jacket with an active coil located very near to the surface of the probe and a second balance coil used to complete the bridge network and provide temperature compensation. The probe is mounted very close to but not touching the target. The target must be an electrically conducting material. The probe then senses the size of the air gap between the face of the probe and the conductive target. As the active coil is excited with AC current, magnetic flux lines from the active coil pass into the conductive target surface. The magnetic flux produces eddy currents in the conducting target which are largest at the target surface and approach zero below the surface. When the gap between the probe and target is lessened, the eddy currents become larger, which changes the impedance of the active coil. The active coil and balance coil form two arms of a bridge circuit whose equivalent impedance varies due to changes in the eddy currents in the target. As the impedance changes, the bridge becomes unbalanced, resulting in an output signal indicative of the gap size. This signal is demodulated and low pass filtered to create a DC signal inversely proportional to the distance being sensed.

The performance of the sensor is very dependent on the properties of the target material. To achieve high performance, the target must have uniform electrical properties, be a good conductor, and should not support a magnetic field. Good target materials are aluminum, copper, and brass. Furthermore, the material must be thick enough to allow the eddy currents to approach zero. The target thickness typically ranges between 0.5 mm to 1.3 mm for different materials.

A differential configuration is often used which allows the two outputs to be subtracted from each other, thus eliminating common mode noise and environmental errors. This requires that the sensor pair and sensor electronics be matched so that they react equally to changes in the environment.

Illustration of Sensor

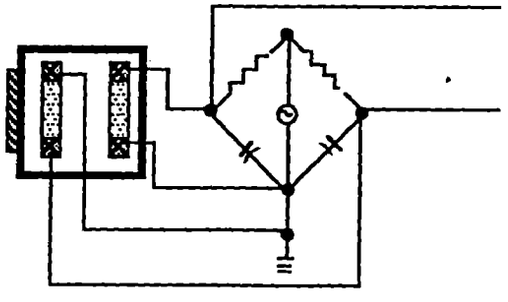

Figure 13.1 Inductive Transducer

Current Industrial Manufacturers

Kaman Instrumentation Measuring Systems
1500 Garden of the Gods Road
Colorado Springs, CO 80907
Telephone: (719) 599-1825
FAX: (719) 599-1823

Bentley, NV
Minden, NV

Current Availability

Available off-the-shelf. SELENE configuration will most likely require custom design.

14. Linear Variable Differential Transformer

Description of Sensor Technology

A linear variable differential transformer (LVDT) consists of a magnetic core or armature, a non-magnetic stem which attaches the core to the object being sensed, and a transformer. The transformer includes a primary coil and two secondary coils surrounded by a magnetic shield. The core moves within the center of the hollow coil without making contact. When the primary coil is excited by an AC voltage, by the principle of mutual inductance, a voltage of the same frequency is induced in both the secondary coils. The amplitudes of the voltages in the secondary coils vary with the core position. When the core is in null position, the amplitudes of the secondary coil outputs are the same. However, for a positive displacement, the voltage amplitude across one secondary coil will increase while the voltage amplitude across the second secondary coil will decrease. In order to produce a single output indicative of the relative core position, the secondary outputs are subtracted; hence, the output goes through a 180° phase shift as the core passes through null. The resulting output is a sin wave whose amplitude is an indication of distance from null, and whose phase is an indication of the direction from null. To create a single DC signal indicating both distance and direction, the output must be demodulated and than filtered. Furthermore, if displacements on either side of null are of interest, phase-sensitive demodulation must be performed. This can be accomplished with a semiconductor diode bridge circuit.

Illustration of Sensor

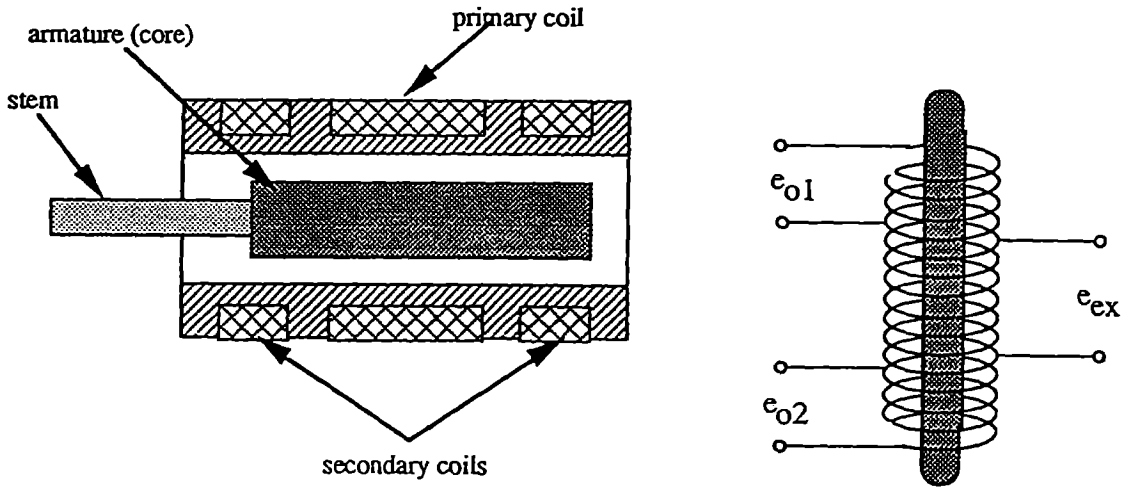

Figure 14.1 Linear Variable Differential Transformer

Mathematical Model of Operating Principles

The LVDT output can be determined by applying circuit analysis to the equivalent circuit below.

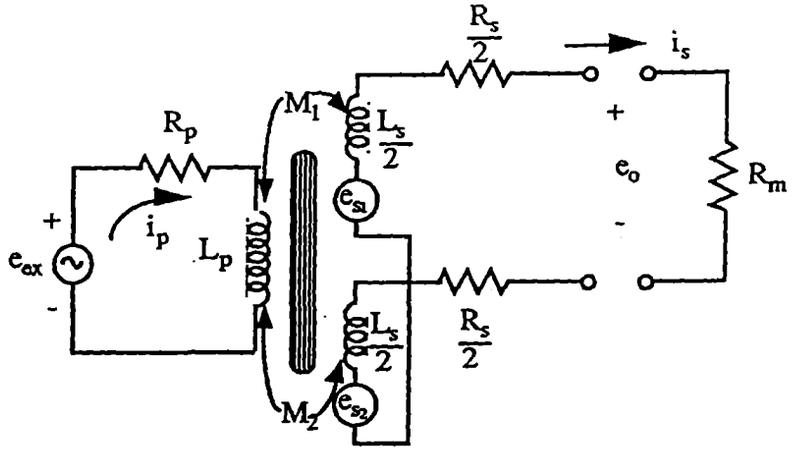

Figure 14.2 LVDT Equivalent Circuit

By applying Kirchhoff's voltage-loop law

$$i_p R_p + L_p \frac{di_p}{dt} - e_{ex} = 0 \tag{14.1}$$

Taking the Laplace transform of Eq. 14.1 and rearranging results in

$$L\left(\frac{di_p}{dt}\right) = \frac{s}{R_p + sL_p} e_{ex} \tag{14.2}$$

Using the notation in Figure 14.2, the voltage induced in each secondary coil is

$$e_{s_1} = M_1 \frac{di_p}{dt} \text{ and} \tag{14.3}$$

$$e_{s_2} = M_2 \frac{di_p}{dt} \tag{14.4}$$

where

M_1, M_2 = respective mutual inductance.

The net output e_s is given by

$$e_s = e_{s_1} - e_{s_2} = (M_1 - M_2)\frac{di_p}{dt} \tag{14.5}$$

It is the values M_1 and M_2 which vary with core position. Therefore, substituting in the expression for di / dt found in Eq. 14.2, at the core null position,

$$e_s = (M_1 - M_2)\frac{s}{L_p s + R_p} e_{ex} \tag{14.6}$$

and thus the transfer function in the Laplace domain is

$$\frac{e_o}{e_{ex}}(s) = \frac{\left[(M_1 - M_2)/R_p\right]s}{\left(L_p/R_p\right)s + 1} \tag{14.7}$$

and the time constant is

$$\tau_p = \frac{L_p}{R_p}. \tag{14.8}$$

The frequency response is determined by setting s = jw, resulting in

$$\frac{e_o}{e_{ex}}(j\omega) = \frac{\omega(M_1 - M_2)/R_p}{\sqrt{(\omega\tau)^2 + 1}} \angle\phi \tag{14.9}$$

where

$$\phi = 90° - \tan^{-1}(\omega\tau_p). \tag{14.10}$$

which proves the 90° phase shift between the input and output.

Current Industrial Manufacturers

Blanchette Tool & Gage Mfg. Corp.
845-T Bloomfield Ave.
Clifton, NJ 07012
Telephone: (201) 471-2100
FAX: (201) 471-2104

Current Availability

Available off-the-shelf. Small sensor with SELENE size and performance requirements will require custom design.

15. Capacitive Transducer

Description of Sensor Technology

A capacitance probe measures the distance (size of the air gap) between the probe and the surface of the target by measuring the capacitance formed by two parallel plates. One plate is the probe surface, while the second plate is the target surface. Capacitance sensors are termed non-contact sensors because no physical contact is required between the sensor and target. A variety of materials can be measured, including metals, dielectrics, and semiconductors. Yet the output is dependent on the material type. All conductive targets affect capacitance the same. However, other material changes require recalibration of the sensor.

Capacitance is dependent on the dielectric constant of the medium in the air gap. The dielectric constant is not only dependent on the media type, but also temperature, pressure, and humidity. Therefore, the capacitance gage accuracy is affected by changes in the above mentioned parameters.

Because the capacitance being measured is typically very small (0.01 - 1.0 pF), stray capacitance which may occur between the sensor and the body must be reduced or eliminated. This can be accomplished through proper shielding and grounding.

The relationship between air gap size and capacitance is not linear, which in some applications may present a problem. A simple op- amp circuit with a sensor in the feedback loop and a fixed capacitor at the positive input can be used to create a linear output.

Other configurations rather than a simple parallel plate combination are possible. The first illustration shows a configuration which measures shear motion between two plates. It is possible for this configuration to be independent of the separation distance between the plates and only indicative of the shear displacement. Furthermore, this arrangement has the advantage that the plate on the target does not need to be powered. The equivalent circuit is two capacitors in series. The second configuration contains two parallel plates which lend themselves well to a bridge network. Bridge networks increase the sensitivity and can be temperature, pressure, and humidity independent when wired properly.[21]

---

[21] Slocum, Alexander H., Massachusetts Institute of Technology. **Precision Machine Design.** Englewood Cliffs, NJ: Prentice Hall; 1992. 750 pages.

Illustration of Sensor

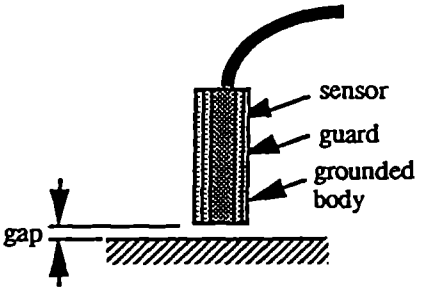

Figure 15.1 Capacitive Transducer

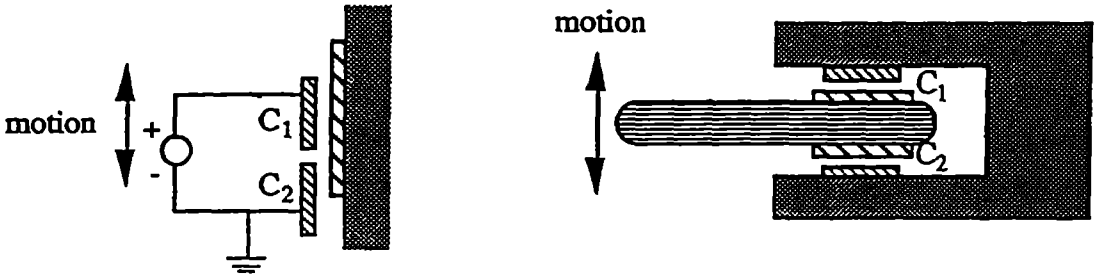

Figure 15.2 Alternative Configurations for a Capacitive Transducer

Mathematical Model of Operating Principles

Capacitance between two parallel plates is

$$C = \frac{\varepsilon A}{x} \tag{15.1}$$

where

C = capacitance between two infinite parallel plates

ε = dielectric constant of the medium in the gap

A = area of the plate, and

d = distance between plates.

From this relationship it can be seen that the input / output relationship is non-linear. Furthermore, it can be seen that any changes in the dielectric constant due to temperature, humidity, or pressure changes will cause a change in the output. The sensitivity of the sensor to changes in distance is found by taking the derivative of the above equation for capacitance with respect to distance. The result is

$$\frac{dC}{dx} = -\frac{\varepsilon A}{x^2}. \tag{15.2}$$

From the above equation it can be seen that the sensitivity increases as the gap size decreases. The output can be linearized with respect to the input with the op-amp circuit below.

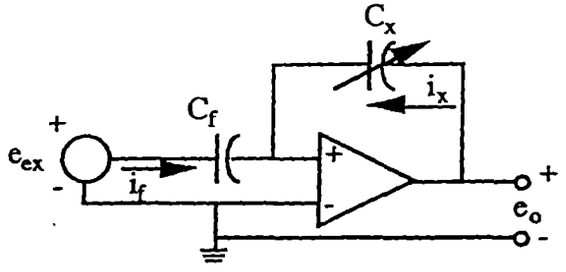

Figure 15.3 Op-Amp Linearization Circuit

Assuming ideal op-amp model, the current going into the positive and negative terminals of the op-amp are zero. Furthermore, the voltage at the negative terminal is 0; therefore the voltage at the positive terminal must also be zero. The result is

$$\frac{1}{C_f}\int i_f dt = e_{ex} \tag{15.3}$$

and

$$\frac{1}{C_x}\int i_x dt = e_0 . \tag{15.4}$$

Since the op-amp draws no current,

$$i_f = -i_x \tag{15.5}$$

and the expression for the output voltage can be rewritten as

$$e_0 = -\frac{1}{C_x}\int i_f dt . \tag{15.6}$$

Substituting

$$\int i_f dt = C_f e_{ex} \tag{15.7}$$

results in a linear relationship between input and output as

$$e_0 = -\frac{C_f}{C_x} e_{ex} . \tag{15.8}$$

Current Industrial Manufacturers

Baumer Electric Ltd.

Kaman Instrumentation Measuring Systems
1500 Garden of the Gods Road
Colorado Springs, CO 80907
Telephone: (719) 599-1825
FAX: (719) 599-1823

Current Availability

Available off-the-shelf. Small sensor with SELENE size and performance requirements will require custom design.

16. Frequency Tracking Fabry-Perot Etalon

Description of Sensor Technology

The Fabry-Perot interferometer consists in its simplest configuration of two slightly wedged transparent plates separated by a distance d. The inner face of each wedge has a semitransparent, highly reflective coating on its surface, and is situated parallel to one another.[22] The outer portion of each wedge is at a slight angle so reflections off this face can be eliminated. The Fabry-Perot interferometer uses multiple beams of light as its source. A single ray of light bounces around numerous times between the two parallel plates. A component of each reflected light is transmitted through the plate and contributes to the interference pattern. In effect, as the light ray bounces around, imperfections in the mirror surface and the non-monochromacity of the light source are averaged out. The result is a very sharp, narrow and bright interference ring pattern.[23]

When the distance between the two parallel plates is kept constant, the device is known as an etalon. The Fabry-Perot etalon (FPE) can be used for distance measurement by frequency tracking methods. Light from a tunable laser is passed through a FPE. The output from the laser is locked onto one of the transmission peaks created by the interference pattern. The locked frequency is then compared to a reference stabilized laser. The frequency difference directly relates to distance changes in the cavity.[24]

Illustration of Sensor

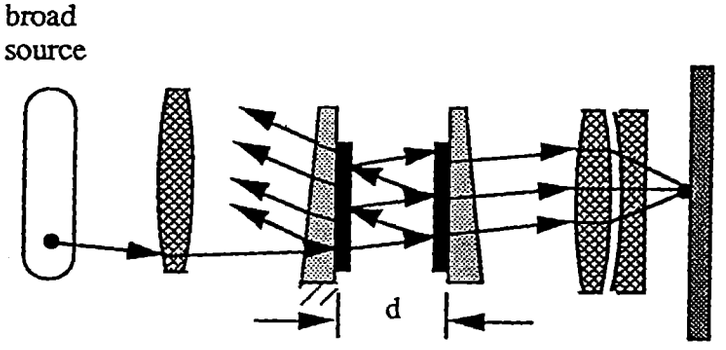

Figure 16.1 *Fabry-Perot Interferometer*

---

[22] Hariharan, P., CSIRO Division of Applied Physics. **Basics of Interferometry.** San Diego, CA: Academic Press, Inc.; 1992. 213 pages.

[23] Slocum, Alexander H., Massachusetts Institute of Technology. **Precision Machine Design.** Englewood Cliffs, NJ: Prentice Hall; 1992. 750 pages.

[24] Teague, C. T. (National Institute of Standards and Technology). **AIP Conference Proceedings 241 Scanned Probe Microscopy.** Wickramasinghe, H. K. *Nanometrology*; 1991; Santa Barbara, CA. ; 1991. 371-407 pages.

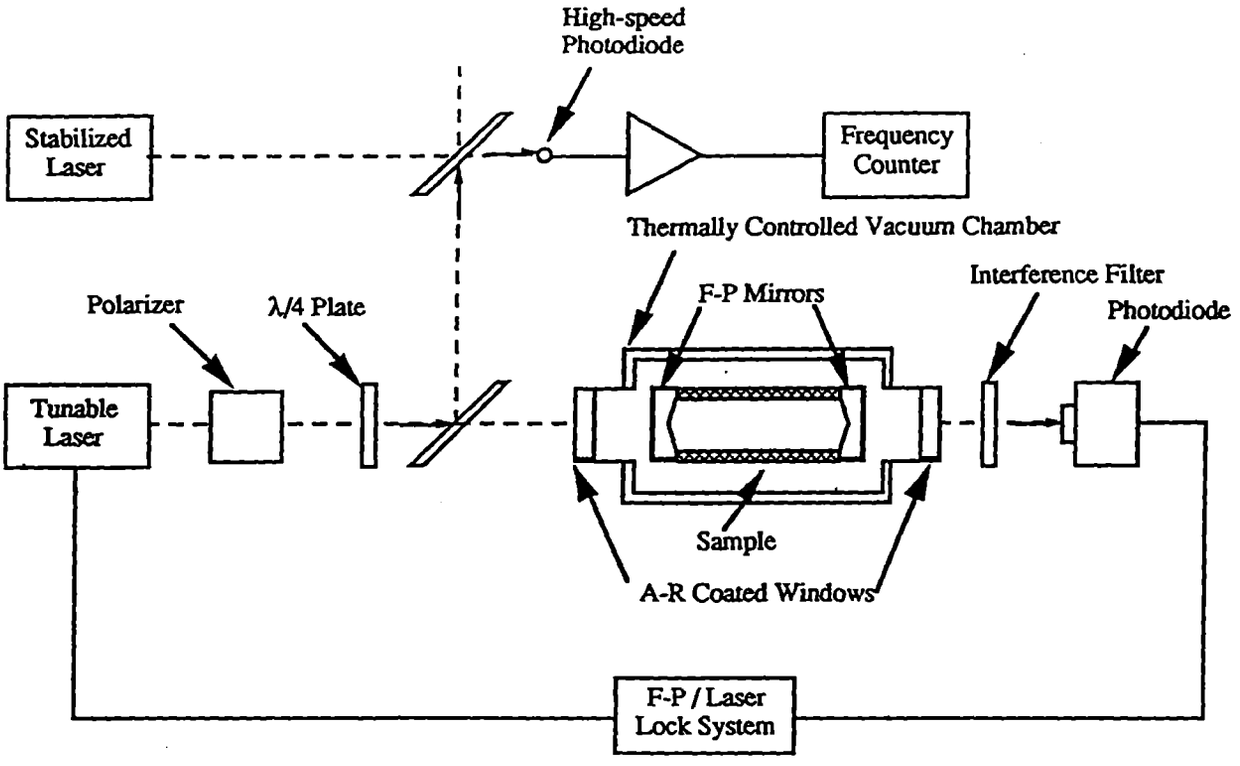

Figure 16.2 Fabry-Perot Etalon

Mathematical Model of Operating Principles

In general, for any interferometer with flat parallel reflecting surfaces, a interference ring pattern is created. Output is maximum when

$$m\lambda_o = 2\mu L\cos\theta \tag{16.1}$$

where

m = order of interference

λ_o = wavelength of radiation

L = effective separation between the two reflecting surfaces

μ = refractive index of the medium in the optical path, and

θ = angle between the reflecting surface normals and direction of source.

The laser is locked on this transmission peak. The change in frequency of a transmission peak due to changes in cavity length can be found from

$$\frac{\partial f}{FSR} = -\frac{\partial L}{\lambda_o/2\mu} \tag{16.2}$$

where

∂f = change in frequency of a transmission peak

FSR = free spectral range of the Fabry-Perot cavity, and

∂L = change in length of cavity.

The FSR is the frequency difference between adjacent modes of the cavity, and can be found from

$$FSR = \frac{c}{2\mu L} \tag{16.3}$$

for parallel plane mirror FPE, where

L = optical length of the cavity.

Current Availability

Not available in configuration appropriate for SELENE edge sensors. Invention necessary.

17. Moiré Metrology

Description of Sensor Technology

When two identical gratings, with one at an incline from the other, are superimposed, the result is an interference pattern termed Moiré fringe. Unlike interferometry, Moiré metrology does not depend on the wave nature of light, thereby requiring a coherent light source. On the contrary, Moiré metrology depends on light only for illumination. The direction of the fringe pattern is perpendicular to the bisector of the angle of rotation between the two grids. The intensity transmitted through the two gratings is proportional to the rotation angle between the grids. As one grid moves with respect to the second grid, the transmitted light pattern will appear to move orthogonally with respect to the direction of motion. Assuming the grid spacing is course in comparison to the wavelength of light, the diffraction effects can be ignored.[25]

Illustration of Sensor

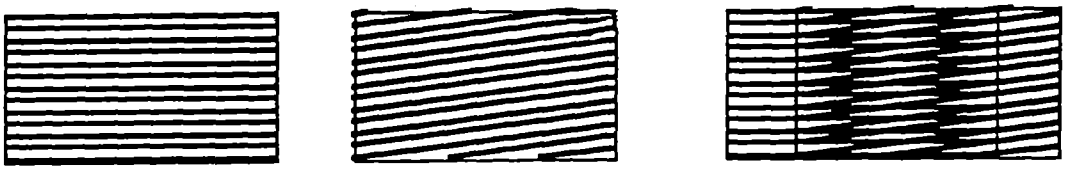

Figure 17.1 Moiré Metrology

Mathematical Model of Operating Principles

In the mathematical analysis, the gratings are replaced by an array of lines.[26]

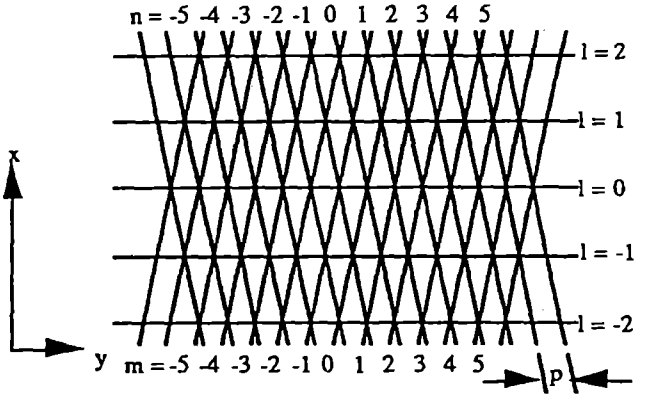

Figure 17.2 Superimposed Array of Lines

---

[25] Slocum, Alexander H., Massachusetts Institute of Technology. **Precision Machine Design.** Englewood Cliffs, NJ: Prentice Hall; 1992. 750 pages.

[26] Kafri, O.; Glatt, I. **The Physics of Moiré Metrology.** New York: John Wiley & Sons; 1990. 194 pages.

A Moiré pattern is formed below by grating G1 and G2, where G1 is -θ/2 from the x axis, and G2 is +θ/2 from the x axis. The gratings are described by

$$y\cos\frac{\theta}{2} = x\sin\frac{\theta}{2} + np \tag{17.1}$$

$$y\cos\frac{\theta}{2} = -x\sin\frac{\theta}{2} + mp \tag{17.2}$$

where

y = position along the y axis

θ = angle between G1 and G2

x = position along the x axis

$n = 0, \pm1, \pm2$, etc. as illustrated

$m = 0, \pm1, \pm2$, etc. as illustrated, and

p = distance between center of gratings along the y axis (pitch).

The points of intersection of the two gratings form an array of fringes whose index is given by

$$l = m - n. \tag{17.3}$$

Substituting for m and n results in

$$l = \frac{2x\sin\theta/2}{p}. \tag{17.4}$$

Rearranging, an expression describing the fringe pattern is

$$x = \frac{lp}{2\sin\theta/2}. \tag{17.5}$$

For small θ, further simplification yields

$$x \approx \frac{lp}{\theta}. \tag{17.6}$$

Similar to the moiré effect, the spacing between bright interference fringes of a wave pattern is described by

$$x = \frac{\lambda}{2\sin\theta/2} \tag{17.7}$$

which again, for small θ, is approximately

$$x \approx \frac{\lambda}{\theta} \tag{17.8}$$

Current Availability Not available in configuration appropriate for SELENE edge sensors. Invention necessary.

18. Hall Effect Transducer

Description of Sensor Technology

When electrons flow through a magnetic field, forces are exerted on the electrons which actually change the path direction of the electrons. This is known as Lorentz's law, and in general Lorentz forces act on any particle moving through a magnetic field. The force is perpendicular to the direction of flow and direction of the magnetic field. When current is flowing through a semiconductor material which is in the presence of a magnetic field, the Lorentz forces act upon the electrons. This is known as the Hall Effect. If the current is perpendicular to the magnetic field, the result is a potential difference perpendicular to both the magnetic field and the current flow. The voltage produced by the Hall Effect is very small, so typically signal conditioning electronics to amplify the output are integrated onto the semiconductor device. This constitutes a solid-state Hall Effect transducer which lends itself to microfabrication techniques of the semiconductor industry.

Hall Effect sensors are very simple and inexpensive. However, they require that a magnet be attached to the target. Typically magnets are not stable devices which further exhibit drift with time. Therefore, these devices are not used in precision sensing situations.[27]

Illustration of Sensor

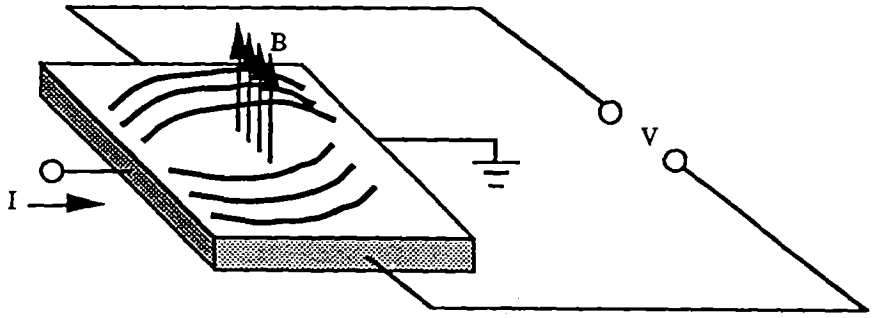

Figure 18.1 Hall Effect Transducer

[27] Slocum, Alexander H., Massachusetts Institute of Technology. **Precision Machine Design.** Englewood Cliffs, NJ: Prentice Hall; 1992. 750 pages.

Current Industrial Manufacturers

Kaman Instrumentation Measuring Systems
1500 Garden of the Gods Road
Colorado Springs, CO 80907
Telephone: (719) 599-1825
FAX: (719) 599-1823

Micro Switch - A Honeywell Division
San Jose Office
4145 North First Street
San Jose, CA 95134-1594
Telephone: (408) 433-3008

Current Availability

Available off-the-shelf. Small sensor with SELENE size and performance requirements will require custom design.

19. Photoelectric Sensor

Description of Sensor Technology

Optical sensing techniques are generally non-perturbing to the measured system, have a very fast response, and have very good resolution. All optical sensors rely on the detection of variances in the basic properties of one or more light beams. These properties are direction of propagation, intensity, wavelength, polarization, and relative phase. These properties are influenced by optical effects such as refraction, reflection, scattering, diffraction, and interference.[28]

An optical sensor based on light intensity (photoelectric sensor) determines range information by transmitting a light source onto the surface being measured. The light diffusely reflects off the surface and is sensed by a receiver. By measuring the intensity of diffusely reflected light, the distance from the sensor to the surface can be determined. A laser is often used as the light source. It is economical and commercially available. However, the sensor performance would be significantly affected if the lens were to become dusty, thereby reducing the amount of reflected light being sensed. Furthermore, this type of sensor does not perform well on surfaces which vary in color or reflectivity.

Illustration of Sensor

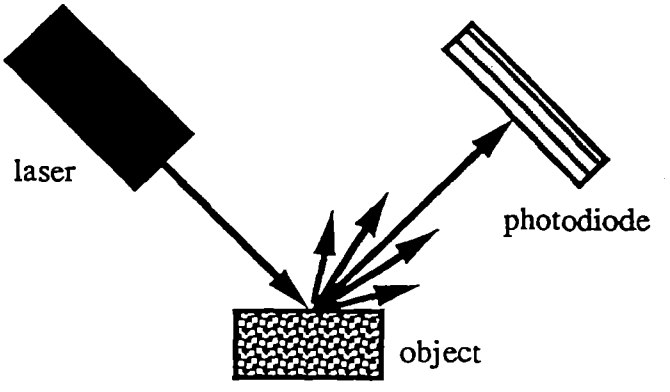

Figure 19.1 Photoelectric Sensor

[28] Nachtigal, C.; Stevenson, W. Modeling and Instrumentation for Physical Systems, ME 385 Course Notes. Purdue University; 1986 Jan. 293 pages.

Current Industrial Manufacturers

Eaton Corporation
Cutler-Hammer Products
4201 North 27th Street
Milwaukee, WI 53216

Banner Engineering Corp.
9716 10th Ave. No.
Minneapolis, MN 55441
Telephone: (612) 546-1333
FAX: (612) 544-3213

Micro Switch
A Honeywell Division
San Jose Office
4145 North First Street
San Jose, CA 95134-1594
Telephone: (408) 433-3008

Current Availability

Available off-the-shelf. Small sensor with SELENE size and performance requirements will require custom design.

20. Laser Triangulation Sensor

Description of Sensor Technology

This optical displacement transducer measures range information using the principle of triangulation. The principle of triangulation determines distance measurements by transmitting a focused laser light source onto an object and then imaging the diffusely reflected light onto a photosensitive device. The photosensitive device (PSD) is an analog light sensor that is sensitive to the intensity and position of a light spot in its field of view. Knowing the position of the image on the PSD, the distance between the detector lens and light source and the projection angle of the source, the distance measurement can be geometrically determined. This type of sensor is commercially available and widely used.

Sensing systems based on triangulation are impervious to color variations. Furthermore, since they measure the location where light is reflected rather than the amount of light being reflected, laser sensors are not sensitive to a dirty environment.

Illustration of Sensor

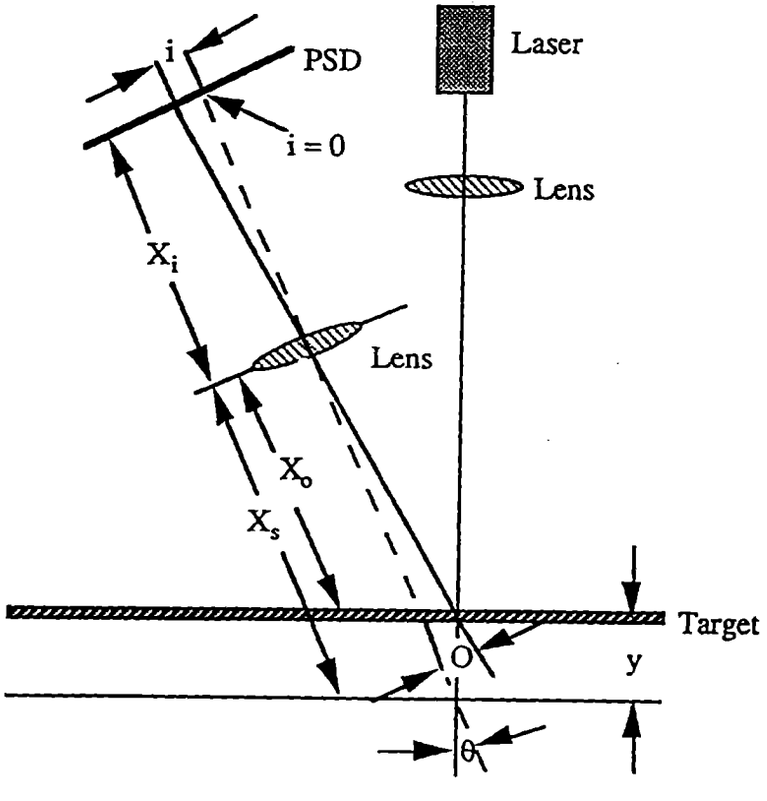

Figure 20.1 Laser Triangulation Sensor

Mathematical Model of Operating Principles

Using the notation shown in Figure 20.1

$$\frac{1}{f} = \frac{1}{X_i} + \frac{1}{X_s} \tag{20.1}$$

where

f = focal length of lens

X_i = fixed distance between lens and image, and

X_s = distance between lens and source.

Rearranging and solving for X_i results in

$$X_i = \frac{fX_s}{X_s - f} . \tag{20.2}$$

By similar triangles,

$$i = \frac{OX_i}{X_o} \tag{20.3}$$

where

O = distance along object from center to image

X_o = object distance from the lens, and

i = distance along photosensitive device from center to image.

Further trigonometric relationships reveal

$$O = y \sin\theta \tag{20.4}$$

and

$$\tan\theta = \frac{O}{X_s - X_o} \tag{20.5}$$

where

X_s = distance between lens and source

θ = angle between transmitter and receiver, and

y = standoff distance, where y = 0 is nominal.

Substitution of Eq. 20.4 into Eq. 20.5 produces

$$\tan\theta = \frac{y \sin\theta}{X_s - X_o} \text{ and} \tag{20.6}$$

$$X_o = X_s - \frac{y \sin\theta}{\tan\theta} . \tag{20.7}$$

Substituting Eq. 20.2 into Eq. 20.3 yields

$$i = \frac{OfX_s}{X_o(X_s - f)}. \tag{20.8}$$

Additionally, substituting Eq. 20.4 into Eq. 20.8 yields

$$i = \frac{y\sin\theta fX_s}{X_o(X_s - f)} \tag{20.9}$$

and substituting Eq. 20.7 into 20.9 gives

$$i = \frac{y\sin\theta fX_s}{(X_s - \frac{y\sin\theta}{\tan\theta})(X_s - f)}, \text{ and} \tag{20.10}$$

$$i = \frac{fX_s}{X_s - f}\frac{y}{\frac{X_s}{\sin\theta} - \frac{y}{\tan\theta}}. \tag{20.11}$$

Because

$$\frac{y}{\tan\theta} << \frac{X_s}{\sin\theta} \tag{20.12}$$

$$i \approx \frac{f}{X_s - f} y\sin\theta. \tag{20.13}$$

As seen by the final equation, the depth measurement y is proportional to the measurement i on the PSD. However, without making the assumption which produced this equation, nonlinearity can be taken into consideration by system static calibration and linearization by common hardware or software signal conditioning schemes.

Current Industrial Manufacturers

Aromat Corporation
Industrial Products Division
629 Central Avenue
New Providence, NJ 07974
Telephone: (800) 228-2350
FAX: (201) 464-8513 or
(201) 464-8714

Perceptron
23855 Research Drive
Farmington Hills, MI 48336
Telephone: (313) 478-7710
FAX: (313) 478-7059

Current Availability

Available off-the-shelf. Small sensor with SELENE size and performance requirements will require custom design.

Table 4 Edge Sensor Technologies[29]

	Resolution (nm)	Accuracy (nm)	Range (nm)	Range Resolution	Max. Rate of Change (nm/s)
Optical Heterodyne Interferometry	0.1	0.1	5×10^7	5×10^8	2.5×10^3
X-Ray Interferometry	5×10^{-3}	10^{-2}	2×10^5	4×10^7	3×10^{-3}
Optical Scales	1.0	5.0	5×10^7	5×10^7	10^6
Inductive Transducers	0.25	—	10^4	2.5×10^5	10^4
LVDT	0.1	—	2.5×10^2	2.5×10^3	$\approx 10^4$
Capacitive Transducers	10^{-3}	—	25	2.5×10^4	10
Fabry-Perot Etalon (Freq. Tracking)	10^{-3}	10^{-3}	5	5×10^3	5 - 10
Moiré Metrology	—	—	—	—	—
Hall Effect Transducer	10^2	—	2.5×10^5 - 3.0×10^7	3.0×10^5	—

[29] Teague, C. T. (National Institute of Standards and Technology). **AIP Conference Proceedings 241 Scanned Probe Microscopy.** Wickramasinghe, H. K. *Nanometrology*; 1991; Santa Barbara, CA. ; 1991. 371-407 pages.